

# Generation of broadband 17- $\mu$ J mid-infrared femtosecond pulses at 3.75 $\mu$ m by silicon carbide crystal

Hai-Tao Fan,<sup>†</sup> Chun-Hua Xu,<sup>†</sup> Zhao-Hua Wang, Gang Wang, Chun-Jun Liu,  
Jing-Kui Liang, Xiao-Long Chen, and Zhi-Yi Wei\*

*Institute of Physics, Chinese Academy of Sciences, South 3rd Street, Zhongguancun,  
Haidian District, Beijing 100190, China*

\*Corresponding author: zywei@iphy.ac.cn

Received September 3, 2014; revised September 29, 2014; accepted September 29, 2014;  
posted September 30, 2014 (Doc. ID 222265); published October 23, 2014

In this contribution, we report the generation of 17- $\mu$ J mid-infrared (MIR) pulses with duration of 70 fs and bandwidth of 550 nm centered at 3.75  $\mu$ m at 1-kHz repetition rate, by a two-stage femtosecond optical parametric amplifier utilizing 4H-silicon carbide crystal as the nonlinear medium. The crystal is selected as it processes orders of magnitude higher damage threshold than traditional MIR nonlinear crystals, and it supports extreme broad parametric bandwidth. With its distinguished features such as MIR central wavelength, ultra-broad bandwidth, self-stable carrier-envelope phase, and potential for energy scaling, this kind of MIR source holds promise for new approaches to extreme short isolated attosecond pulse generation as well as MIR spectroscopy applications. © 2014 Optical Society of America

OCIS codes: (190.4970) Parametric oscillators and amplifiers; (320.7110) Ultrafast nonlinear optics.  
<http://dx.doi.org/10.1364/OL.39.006249>

Mid-infrared (MIR) light sources in the molecular “fingerprint” region are of particular importance in a number of disciplines, including industrial process monitoring, environmental monitoring, and molecular identification [1]. Driven by intense carrier-envelope phase-stable MIR pulses, high-order harmonic generation process exhibits higher cut-off energy, supporting shorter isolated attosecond pulses [2]. Broadband MIR light sources are also essential in optical coherence tomography [3,4], since broad spectrum leads to ultrahigh resolution and longer wavelength results in better penetration depth.

As MIR light sources have widespread applications, several approaches are made to obtain laser radiations at this wavelength region. Lead-salt diodes exhibit two orders of magnitude lower Auger recombination rate compared with other materials, but they are hindered in applications by a low working temperature requirement, especially for continuous wave operation [5,6]. Unlike lead-salt lasers, the main nonradiative channel for quantum cascade lasers [7,8] is optical phonon emission rather than the Auger effect. That offers opportunities for room temperature operation. However, quantum cascade lasers suffer from their low wall plug efficiency, which sets limitation to applications such as portable sensors and infrared counter measurements [9]. Additionally, generation of lasers with wavelength longer than 3  $\mu$ m based on solid-state lasers is limited by the multiphonon relaxation process in gain media at room temperature [10].

Different from the laser radiation obtained by stimulated emission process mentioned above, nonlinear frequency conversion techniques as the third-generation femtosecond technology [11] have been developed to acquire MIR pulses. By utilizing virtual energy levels for amplification, they are free of cooling systems as no energy accumulates inside the gain media. Among these techniques, optical parametric amplification (OPA) [12–18], owing to its distinguished advantages including ultra-broad parametric bandwidth and ultrahigh gain per

pass, has become an ideal way to generate MIR pulses, compared with other nonlinear processes [19–25].

A series of nonlinear crystals are employed to serve in these systems. Crystals like AgGaS<sub>2</sub> [26] and ZnGeP<sub>2</sub> [27] have transparency to the far-infrared region and satisfy phase matching condition near or beyond 10  $\mu$ m. Meanwhile, periodically poled crystals such as MgO:PPLN [16,20] and PPSLT [13] usually possess large nonlinear coefficients, leading to high conversion efficiency. However the final output MIR pulse energy from these crystals are hindered by their limited apertures. None of these MIR nonlinear crystals possesses damage threshold over 1 GW/cm<sup>2</sup>.

4H-silicon carbide (4H-SiC) crystal, belonging to 6-mm point group, is a kind of positive uniaxial crystal. It exhibits two intrinsic superiorities in intense few-cycle MIR pulse generation. First, it possesses orders of magnitude higher damage threshold (80 GW/cm<sup>2</sup>) [28] than traditional MIR nonlinear crystals partly because of its strong C-Si covalent bond. Second, based on the Sellmeier equations of 4H-SiC crystal [29], type II phase matching condition can be satisfied [Fig. 1(a)]. Pumped by 800-nm pulses, 4H-SiC shows intrinsic ultra-broad parametric bandwidth when the phase matching angle (PMA) is close to 90°. Besides the bandwidth concern, 90° PMA is selected to avoid walk-off effect [Fig. 1(a) inset] and to easily polish the crystal with high angular accuracy. Broadband parametric amplification can only be achieved when group velocities of the signal and the idler are matched. Figure 1(b) shows group velocity mismatch (GVM) and corresponding idler parametric bandwidth for different noncollinear angle when signal wavelength is centered around 1  $\mu$ m. A slight noncollinear scheme is intentionally employed to make sure that signal wave and idler wave temporally overlap each other throughout the crystal. Ultrabroad parametric bandwidth of more than 500 nm for idler wave can be obtained theoretically utilizing optimized noncollinear angle. The angular dispersion (AD) of the idler from a noncollinear optical

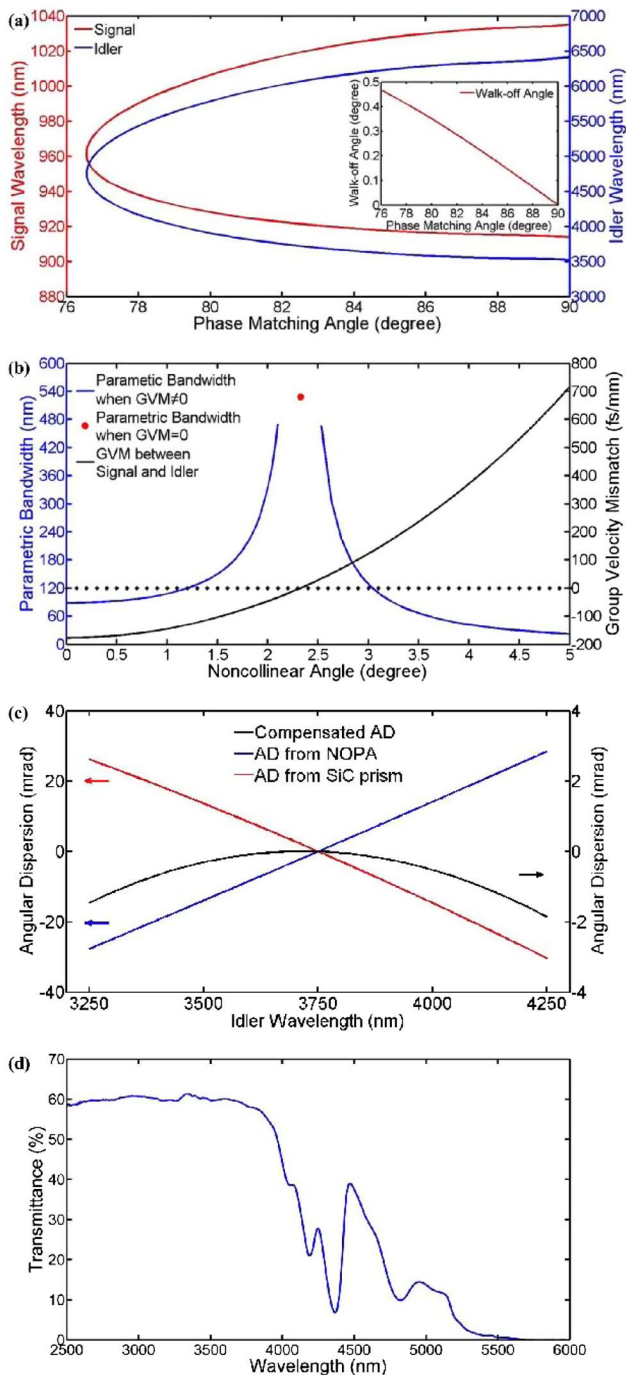


Fig. 1. Characteristics of 4H-SiC crystal. (a) Type II phase matching curve of 4H-SiC crystal (inset: walk-off angle for different phase-matching angle). (b) Calculated group velocity delay between signal and idler wave, and corresponding parametric bandwidth for the idler. (c) Angular dispersion introduced by NOPA and its compensation by a 4H-SiC prism (d) Transmittance of 3-mm-thick 4H-SiC crystal from 2.5 to 6  $\mu\text{m}$ .

parametric amplifier (NOPA) can not be avoided. As 2.3° noncollinear angle is set for bandwidth concern, the AD is calculated to be 52 mrad throughout the MIR spectrum (from 3250 to 4250 nm). The blue line in Fig. 1(c) indicates that the AD is approximately linear, since the noncollinear angle is relatively small. That offers opportunities to compensate it by use of a 4H-SiC prism, which

gives also nearly linear AD when working at minimum deviation angle [Fig. 1(c), red line]. After the compensation of a prism with optimized 41° apex angle, the AD of the idler can be reduced to less than 2 mrad throughout the whole 1000-nm-wide MIR spectrum [Fig. 1(c), black line]. As a key parameter of the crystal used as gain medium, the transmittance can directly influence the energy efficiency of OPA system. By utilizing Fourier transform infrared spectrometer (FTS-60V), transmission rate of 4H-SiC crystal [Fig. 1(d)] is obtained and it exhibits high transmittance below 4  $\mu\text{m}$ . In fact, as one of our previous works, femtosecond MIR pulses generated by difference frequency generation (DFG) process using 4H-SiC has been reported [29].

The experimental setup illustrated in Fig. 2 consists of two stages of NOPAs and a sum-frequency generation stage used for pulse width characterization. A home-built Ti:sapphire regenerative amplifier, which delivers laser pulses with 1.8-mJ energy and 52-fs duration (measured by a commercial single shot auto-correlator Everfsmeter, Daheng Inc.) at 1 kHz repetition rate, is utilized as the pump source. A 50:50 beam splitter is placed to separate the pump beam into two parts with same pulse energy. One half of the 800-nm pump pulses is frequency doubled by a 1-mm-thick BBO crystal ( $\varphi = 29.2^\circ$ ,  $\phi = 0^\circ$  CASTECH Inc. Fujian). Laser energy of 250  $\mu\text{J}$  is generated at 400-nm wavelength to pump the first stage of NOPA. The energy of residual 800-nm laser pulses is adjusted by a combination of a half-wave plate and a Glan-prism and focused on a 2-mm-thick undoped YAG plate to generate single filament white light continuum (WLC). The 1- $\mu\text{m}$  component of the WLC spectrum is amplified to 15  $\mu\text{J}$  with approximately 60-nm bandwidth [Fig. 3(a)] by utilizing a 3-mm-thick type I BBO crystal ( $\varphi = 28.6^\circ$ ,  $\phi = 0^\circ$  CASTECH Inc. Fujian) in the first stage, accompanied by the appearance of bright signal pulses centered around 660 nm. After the first stage of NOPA, the 1- $\mu\text{m}$  part pulses are collimated and fed into the second stage, in which a 3-mm-thick type II 4H-SiC crystal ( $\varphi = 90^\circ$ ,  $\phi = 0^\circ$  Tankeblue Co. Ltd., Beijing) is used for parametric amplification. An optimized 2.3° noncollinear angle

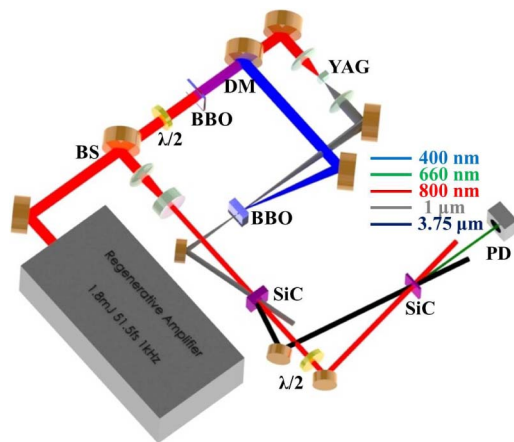


Fig. 2. Schematic layout of two-stage NOPA system and sum-frequency generation stage. (Delay line ignored) BS, beam splitter;  $\lambda/2$ , half-wave plate; DM, dichroic mirror; PD, photo diode

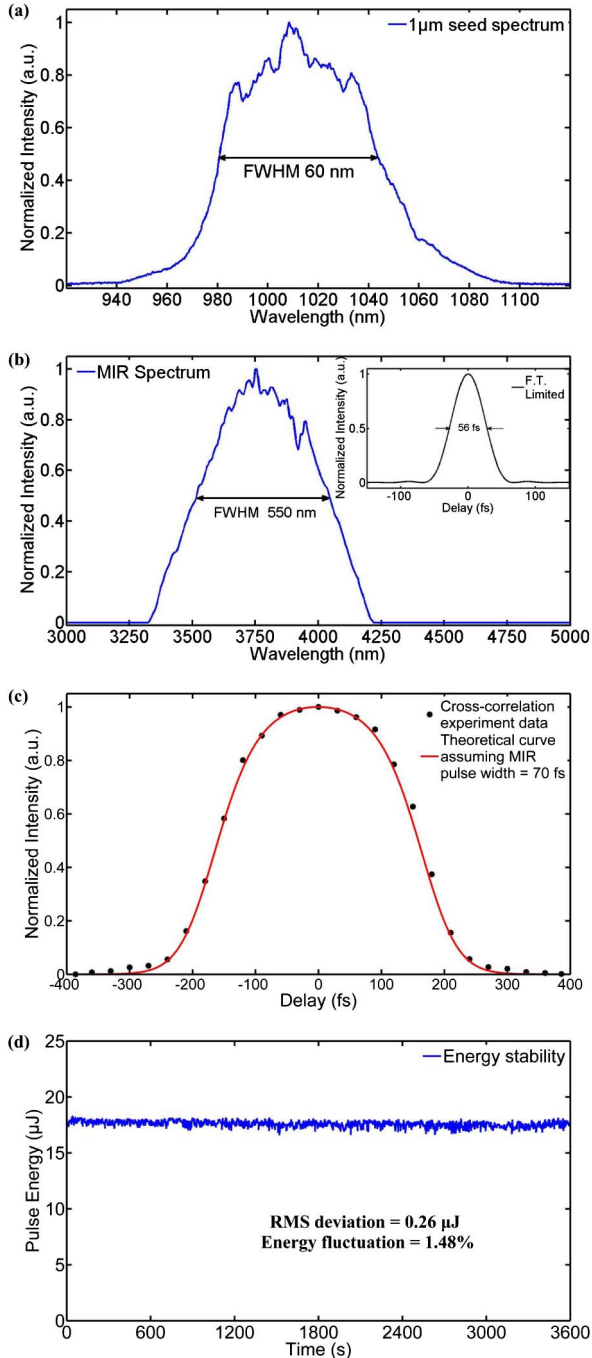


Fig. 3. Experiment results. (a) 1- $\mu\text{m}$  seed spectrum of the second NOPA, (b) MIR spectrum (inset: corresponding FT Limited pulse). (c) Intensity distribution of cross-correlation signal at 660 nm (points: experiment data, line: calculated cross-correlation intensity between 52-fs near infrared pump pulses and 70-fs MIR pulses). (d) Energy stability of MIR pulses.

calculated above is employed in order to achieve ultra-broadband parametric amplification. The beam size of the pump and the signal is matched at around 1.5 mm throughout the crystal, corresponding to nearly  $1 \text{ GW}/\text{cm}^2$  intensity. Pumped by 900- $\mu\text{J}$  laser pulses at 800 nm, the energy of signal is boosted from 15  $\mu\text{J}$  to more than 130  $\mu\text{J}$  with bandwidth of approximately 40 nm, generating 17- $\mu\text{J}$  idler pulses on the other side

of the pump pulses at 3.75  $\mu\text{m}$  simultaneously. The spectrum of the MIR idler, shown in Fig. 3(b), is acquired by a monochromator (Omni- $\lambda$  150, Zolix Instruments Ltd.) combined with an HgCdTeZn infrared detector (Vigo System) and DSP lock-in amplifier (SR830 Stanford Research Systems). Centered at 3.75  $\mu\text{m}$ , the spectrum has an extremely broad bandwidth of 550 nm (full width at half-maximum, FWHM), which is consistent with the theoretical results in Fig. 1(b). That spectrum supports Fourier Transform limited (FT Limited) pulses with 56-fs pulse duration [Fig. 3(b), inset], assuming hyperbolic secant electric field distribution.

An additional sum-frequency generation stage is built to illustrate the temporal character of MIR pulses. The residual 800-nm pump pulses after the second NOPA pass through a half-wave plate to change its polarization. Meanwhile the MIR pulses go through a 2-mm-thick germanium plate to filter pulses with shorter wavelength and to partly compensate the dispersion, as germanium has roughly the same amount but opposite sign of second-order dispersion compared with 4H-SiC crystal at 3.75- $\mu\text{m}$  region. Bright cross-correlation signal centered at 660 nm appears when the near-infrared and MIR pulses overlap temporally and spatially in a 1-mm-thick 4H-SiC crystal ( $\varphi = 90^\circ$ ,  $\phi = 0^\circ$  Tankeblue Co. Ltd., Beijing). The intensity distribution of cross-correlation signal depends mainly on the GVM between two pulses with fundamental frequencies, and their pulse durations [30]. The experimental data of the intensity distribution of 660-nm cross-correlation signal is obtained by scanning the time delay between two pulses with fundamental frequencies. Illustrated in Fig. 3(c), they match well with theoretical line with the assumption of 70-fs MIR pulse duration, indicating the electric field oscillates only six cycles within the FWHM intensity. In addition, the energy stability of MIR pulses is measured to be 1.48% (RMS) within 1 h [Fig. 3(d)].

In conclusion, we have theoretically illustrated the optical character of 4H-SiC crystal as an ideal parametric medium for intense few-cycle MIR pulse generation in OPA system, and experimentally demonstrated a two-stage NOPA system delivering 17- $\mu\text{J}$ , 70-fs MIR pulses with 550-nm bandwidth centered at 3.75  $\mu\text{m}$  at 1-kHz repetition rate. Additionally, the MIR pulses, generated by difference frequency between two near-infrared pulses derived from the same source, are expected to have a stable carrier-envelope phase [31], which is crucial in strong field physics and extreme short isolated attosecond pulses generation.

This work is partially supported by the National Key Basic Research Program of China under Grant No. 2013CB922402 and National Natural Science Foundation of China under Grant No. 51272276. The authors thank Nan Wang, Peng Ye, and Zhong-Wei Shen for helpful discussions on theoretical analysis of OPA process. We are also in debt Shun-Chong Wang and Min-Jie Zhan for assistance in crystal property measurements and OPA results acquisition, respectively. C. H. X., G. W., and X. L. C. thank F. Y. and Z. Y. X. of Technical Institute of Physics and Chemistry CAS for helpful discussions.

<sup>†</sup>These authors contribute equally to this work.

## References

1. K. P. Petrov, R. F. Curl, and F. K. Tittel, *Appl. Phys. B* **66**, 531 (1998).
2. T. Popmintchev, M. C. Chen, D. Popmintchev, P. Arpin, S. Brown, S. Alisauskas, G. Andriukaitis, T. Balciunas, O. D. Mucke, A. Pugzlys, A. Baltuska, B. Shim, S. E. Schrauth, A. Gaeta, C. H. Garcia, L. Plaja, A. Becker, A. J. Becker, M. M. Murnane, and H. C. Kapteyn, *Science* **336**, 1287 (2012).
3. C. S. Colley, J. C. Hebden, D. T. Delpy, A. D. Cambrey, R. A. Brown, E. A. Zibik, W. H. Ng, L. R. Wilson, and J. W. Cockburn, *Rev. Sci. Instrum.* **78**, 123108 (2007).
4. B. Guo, Y. Wang, C. Peng, H. L. Zhang, G. P. Luo, and H. Q. Le, *Opt. Express* **12**, 208 (2004).
5. Z. Feit, M. McDonald, R. J. Woods, V. Archambault, and P. Mak, *Appl. Phys. B* **68**, 738 (1996).
6. M. Tacke, *Phil. Trans. R. Soc. A* **359**, 547 (2001).
7. J. Faist, F. Capasso, D. L. Sivco, C. Sirtori, A. L. Hutchinson, and A. Y. Cho, *Science* **264**, 553 (1994).
8. J. Faist, F. Capasso, C. Sirtori, D. L. Sivco, J. N. Baillargeon, A. L. Hutchinson, S. G. Chu, and A. Y. Cho, *Appl. Phys. Lett.* **68**, 3680 (1996).
9. Y. Yao, A. J. Hoffman, and C. F. Gmachl, *Nat. Photonics* **6**, 432 (2012).
10. E. Sorokin, S. Naumov, and I. T. Sorokina, *IEEE J. Sel. Top. Quantum Electron.* **11**, 690 (2005).
11. H. Fattahi, H. G. Barros, M. Gorjan, T. Nubbemeyer, B. Alsaif, C. Y. Teisset, M. Schultze, S. Prinz, M. Haefner, M. Ueffing, A. Alismail, L. Vamos, A. Schwarz, O. Pronin, J. Brons, X. T. Geng, G. Arisholm, M. Ciappina, V. S. Yakovlev, D. E. Kim, A. M. Azzeer, N. Karpowicz, D. Sutter, Z. Major, T. Metzger, and F. Krausz, *Optica* **1**, 45 (2014).
12. T. M. Jedju and L. Rothberg, *Appl. Opt.* **26**, 2877 (1987).
13. D. Brida, M. Marangoni, C. Manzoni, S. D. Silvestri, and G. Cerullo, *Opt. Lett.* **33**, 2901 (2008).
14. G. Andriukaitis, T. Balciunas, S. Alisauskas, A. Pugzlys, A. Baltuska, T. Popmintchev, M. C. Chen, M. M. Murnane, and H. C. Kapteyn, *Opt. Lett.* **36**, 2755 (2011).
15. X. P. Liu, R. M. Osgood, Jr., Y. A. Vlasov, and W. M. J. Green, *Nat. Photonics* **4**, 557 (2010).
16. C. Erny, C. Heese, M. Haag, L. Gallmann, and U. Keller, *Opt. Express* **17**, 1340 (2009).
17. D. Brida, C. Manzoni, G. Cirimi, M. Marangoni, S. Bonora, P. Villoresi, S. D. Silvestri, and G. Cerullo, *J. Opt.* **12**, 013001 (2010).
18. X. Gu, G. Marcus, Y. Deng, T. Metzger, C. Teisset, N. Ishii, T. Fuji, A. Baltuska, R. Butkus, V. Pervak, H. Ishizuki, T. Taira, T. Kobayashi, R. Kienberger, and F. Krausz, *Opt. Express* **17**, 62 (2009).
19. K. C. Burr, C. L. Tang, M. A. Arbore, and M. M. Fejer, *Opt. Lett.* **22**, 1458 (1997).
20. J. Liu, Q. Liu, X. Yan, H. Chen, and M. Gong, *Laser Phys. Lett.* **7**, 630 (2010).
21. L. Goldberg, W. K. Burns, and R. W. McElhanon, *Opt. Lett.* **20**, 1280 (1995).
22. C. Erny, K. Moutzouris, J. Biegert, D. Kuhlke, F. Adler, A. Leitenstorfer, and U. Keller, *Opt. Lett.* **32**, 1138 (2007).
23. I. Galli, S. Bartalini, S. Borri, P. Cancio, G. Giusfredi, D. Mazzotti, and P. D. Natale, *Opt. Lett.* **35**, 3616 (2010).
24. H. Xuan, Y. Zou, S. Wang, H. Han, Z. Wang, and Z. Wei, *Appl. Phys. B* **108**, 571 (2012).
25. T. Fuji and T. Suzuki, *Opt. Lett.* **32**, 3330 (2007).
26. Y. X. Fan, R. C. Eckardt, R. L. Byer, R. K. Route, and R. S. Feigelson, *Appl. Phys. Lett.* **45**, 313 (1984).
27. G. D. Boyd, E. Buehler, and F. G. Storz, *Appl. Phys. Lett.* **18**, 301 (1971).
28. S. Niedermeier, H. Schillinger, R. Sauerbrey, B. Adolph, and F. Bechstedt, *Appl. Phys. Lett.* **75**, 618 (1999).
29. S. Wang, M. Zhan, G. Wang, H. Xuan, W. Zhang, C. Liu, C. Xu, Y. Liu, Z. Wei, and X. Chen, *Laser Photon. Rev.* **7**, 831 (2013).
30. D. C. Edelstein, E. S. Wachman, L. K. Cheng, W. R. Bosenberg, and C. L. Tang, *Appl. Phys. Lett.* **52**, 2211 (1988).
31. A. Baltuska, T. Fuji, and T. Kobayashi, *Phys. Rev. Lett.* **88**, 133901 (2002).